Potential of Microchannel Flow for Agglomerate Breakage

J. J. Derksen*,† and D. Eskin‡

Chemical & Materials Engineering, University of Alberta, Edmonton, AB, T6G 2G6 Canada, and Schlumberger DBR Technology Center, Edmonton, AB, T6N 1M9 Canada

Direct simulations of laminar solid−liquid flow in microchannels with full resolution of the solid−liquid interfaces have been performed. The solids phase consists of simple agglomerates, assembled of monosized, spherical particles. The flow of the interstitial liquid is solved with the lattice-Boltzmann method. Solids and fluid dynamics are two-way coupled. The simulations keep track of the flow-induced forces in the agglomerates. The effects of agglomerate type (doublets, triplets, and quadruplets), solids loading, and channel geometry on (the statistics of the) flow and collision-induced forces has been investigated. By comparing these forces with agglomerate strength, we would be able to assess the potential of microchannels as agglomerate breakage devices.

Introduction

In many processes involving solid particle formation or solids handling, particles have a tendency to stick together. In crystallization processes, crystals tend to agglomerate due to the supersaturated environment they are in.[1,2] Suspension polymerization processes go through a "sticky-phase" with significant agglomeration levels.[3] In colloidal systems, a variety of interactions can cause agglomeration (related to van der Waals forces, electrolyte-induced interactions, surface chemistry),[4] and stabilization of colloids is a central issue. In biorelated applications, agglomeration plays a role in such diverse fields as blood flow[5] and biomolecular cross-linking of particles.[6] The application which is driving the present research is the behavior of asphaltenes, more specifically their deposition on walls in oil reservoirs (Boek et al.[7] and references therein). Asphaltene agglomeration is a key step in asphaltene deposition since the agglomerate size and the agglomerate sticking probability to the wall are intimately related: only relatively small agglomerates stick to the wall while bigger ones are removed with the flow. The agglomerate size distribution evolves as a result of agglomeration and also deagglomeration (i.e., breakage of agglomerates). According to recent work on asphaltene particle size distributions in a Couette laminar flow,[8] asphaltene particles can be considered as solid particles of nonspherical shapes (having a fractal dimension smaller than three).

For an agglomeration event to occur, particles (primary particles and/or agglomerates) need to collide first. Typically collisions are induced by Brownian motion, gravity, and velocity gradients in the fluid carrying the particles since these phenomena bring about relative velocities between particles. Also particle inertia can be a source of collisions.

Next to promoting collisions, fluid velocity gradients and particle−particle interactions are potential reasons for agglomerate breakage since they cause mechanical loads on agglomerates. In this paper, we focus on the latter aspect: We investigate the mechanical load on agglomerates due to deformation of the surrounding liquid and the presence of other particles/agglomerates. Interactions with other particles/agglomerates can be either direct (collisions) or indirect, e.g. transmitted by the interstitial liquid.

In modeling processes involving agglomeration, population balances are often used to keep track of agglomerate size distributions.[8−10] In order to equip population balances with adequate agglomeration and breakage physics, rate laws (usually termed kernel functions) are being developed that relate numbers of agglomeration and breakage events per unit volume and time to local (flow and agglomerate) conditions. With the purpose of devising kernels, there is extensive literature on agglomeration and breakage as a result of hydrodynamics for small (though non-Brownian) agglomerates in turbulent flow (see ref 13 and references therein). Small in this context means that the agglomerate size is significantly smaller than the smallest dynamical scale of turbulence, i.e. the Kolmogorov scale. If this is the case the flow field surrounding the agglomerate can be assumed to scale with the (local) rate of energy dissipation and be of some canonical, simple nature, and disruptive forces, as well as collision probabilities can be modeled fairly accurately based on Stokes flow principles (see e.g. the works of Nir and Acrivos,[12] Bäbler et al.[13]). In a previous paper,[11] however, it was argued that the situation significantly complicates if the agglomerate (in that paper a doublet of spheres) has a size of the same order as the Kolmogorov scale, or is larger. It then experiences an inhomogeneous flow, and the (fluctuating) details of the hydrodynamics around it are crucial for its internal forces and thus breakage probability. A similar situation occurs in microreactor equipment where (as an example) agglomerate slurries are being sent through nozzle-shaped microchannels to facilitate breakage.[14,15] Again, there is a nontrivial flow field around the agglomerate that induces internal forces that can break it.

From the above, it may be clear that information regarding flow-induced and particle-interaction-induced forces in agglomerates is a key in describing their probability to break. In this paper, a computational procedure is presented to determine these forces from first principles. In the computations, agglomerates are assembled of primary spherical particles all having the same size and released in a flow field. We directly solve the flow around the agglomerates and fully couple flow and agglomerate motion. The force and torque required to keep a primary particle attached to the agglomerate follow from this computational procedure. Comparing that force and/or torque with a measure of the agglomerate strength allows for assessing the breakage probability. Usually a primary sphere has more than one contact point with the other primary spheres in the

* To whom correspondence should be addressed. E-mail: jos@ualberta.ca.
† University of Alberta.
‡ Schlumberger DBR Technology Center.

10.1021/ie100442e

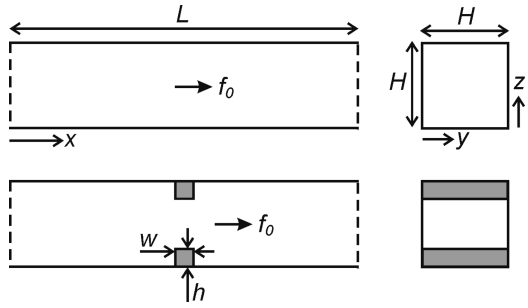

Figure 1. Definition of the flow channel and coordinate system. (top panels) Uniform channel; (bottom panels) Channel with contraction. In the streamwise (x) direction, periodic conditions apply.

agglomerate. This (in general) makes it fundamentally impossible to calculate the force and torque at each contact point. However, for a few simple agglomerate configurations, the force and torque per contact point can be determined with minimal assumptions.

It should be noted that during the simulations presented in this paper the agglomerates keep their integrity and shape; we do not actually break them. In that sense, the present work differs from computational work due to Higashitani et al.,[16] where agglomerates are actually broken, and from more recent works,[17,18] which focus on flow-induced restructuring of complex agglomerates with, however, much simpler representations of the hydrodynamic environments of the agglomerates.

The results of our simulations comprise detailed representations (time series, probability density functions) of the flow-induced forces and torques in agglomerates as a function of process conditions. From this detailed information, the breakage probability can be assessed once data regarding the mechanical strength of the specific agglomerates at hand is available.

In this paper, we first define the flow systems in terms of their dimensionless parameters, and indicate which part of the parameter space we will be exploring. Then the computational framework for calculating the flow-induced forces in agglomerates is explained. We then apply the method to flow of agglomerate slurries in microchannels where we compare forces in different types of simple agglomerates, viz. doublets, triplets arranged in triangles, and quadruplets arranged in tetrahedrons, all made of equally sized spherical particles. By considering a range of solids volume fractions of the agglomerate slurries, the role of particle−particle interactions on the mechanical load on agglomerates is assessed. Furthermore, a few different microchannel layouts have been compared. Specifically we compare straight, square channels with channels having contractions.

Flow System Definitions and Parameter Space

The basic flow geometry in this study is a square channel; see Figure 1 for a definition of its dimensions and coordinate system. The flow in the channel is driven by a body force f_0 acting in the x (= streamwise) direction mimicking a pressure gradient (or, if vertically placed, gravity). At the four side walls, a no-slip boundary condition applies; the system is periodic in the streamwise direction. A Reynolds number characterizing the flow in the channel can be based on the wall shear velocity $u_\tau = \sqrt{\tau_w/\rho}$: $Re_w = u_\tau H/\nu$ with ν the kinematic viscosity of the liquid in the channel and ρ its density. The average wall shear stress τ_w follows from an overall force balance: $4H\tau_w = H^2 f_0$ so that eventually

$$Re_w = \frac{1}{2}\frac{H^{3/2} f_0^{1/2}}{\rho^{1/2}\nu} \tag{1}$$

Inspired by work due to Zaccone et al.[14] and Soos et al.,[15] in some of the simulations the channel has a contraction as defined in the bottom panels of Figure 1. The contraction is two-dimensional, i.e. the channel is only contracted locally in the z-direction; the width in the y-direction remains H. The Reynolds number definition for the contracted channel cases is the same as for the uniform channel, i.e. eq 1. All channels considered have a length-over-width aspect ratio $L/H = 2.0$.

In the liquid that fills the channel, agglomerates are released. They consist of equally sized spheres with radius a. Three types of agglomerates will be considered: (1) two touching spheres forming a doublet; (2) three touching spheres (triplet) forming a triangle (two contact points per primary sphere); (3) four touching spheres (quadruplet) forming a tetrahedron (three contact points per primary sphere). The introduction of the agglomerates in the channel gives rise to three additional dimensionless numbers: an aspect ratio a/H, a density ratio ρ_s/ρ, and a solids volume fraction ϕ. The density ratio is relevant with a view to inertial effects, e.g. related to slip velocities and particle−particle and particle−wall collisions. We do not consider gravity in the simulations; it is assumed that $(\rho_s - \rho)g/f_0 \ll 1$.

In this paper, only part of the parameter space as identified above has been explored; Re_w, a/H, and ρ_s/ρ have been fixed to values 2.6, 0.05, and 2.5, respectively (this density ratio is e.g. representative of glass beads in a watery liquid). We consider three solids volume fractions $\phi = 0.031$, 0.062, and 0.093; three different types of agglomerates doublets, triplets, and quadruplets; and three different flow geometries a uniform channel ($h/H = 0$; see Figure 1) and two channels with contractions having $h/H = 0.2$ and 0.3. In all contracted channels, $w/L = 0.1$.

Simulation Procedure

In the simulations, a number of agglomerates made of equally sized spheres (primary spheres) are placed in the liquid filled domain. The motion of the agglomerates and the liquid are fully coupled, i.e. the fluid flow sets the agglomerates in motion; the motion of the agglomerates on its turn induces fluid flow. The fluid flow we solve with the lattice-Boltzmann method (LBM). For flows in complexly shaped domains and/or with moving boundaries, this method has proven its usefulness (see e.g. the review article by Chen and Doolen[19]). In the LBM, the computational domain is discretized into a number of lattice nodes residing on a uniform, cubic grid. Fluid parcels move from each node to its neighbors according to prescribed rules. It can be proven by means of a Chapman−Enskog expansion that, with the proper grid topology and collision rules, this system obeys, in the low Mach number limit, the incompressible Navier−Stokes equations.[19,20] The specific implementation used in our simulations has been described by Somers,[21] which is a variant of the widely used lattice BGK scheme to handle the collision integral (e.g., see the work of Qian et al.[22] for a detailed discussion of LBGK). We use the scheme due to Somers, as it manifests a more stable behavior at low viscosities when compared to LBGK. A lattice-Boltzmann fluid is a compressible fluid. In order to mimic incompressible flow, as is done in this paper, the Mach number must be sufficiently low. In the simulations presented here, the local Mach number never exceeded 0.05.

The fluid flow and the motion of the agglomerates are coupled by demanding that at the surface of each primary sphere the fluid velocity matches the local velocity of the solid surface (that is the sum of the linear velocity $\mathbf{v}_a$ and $\boldsymbol{\omega}_a \times (\mathbf{r} - \mathbf{r}_a)$ with $\boldsymbol{\omega}_a$ being the angular velocity of the agglomerate the primary sphere is part of, $\mathbf{r}_a$ is the agglomerate's center of mass, and $\mathbf{r}$ is a point on the primary sphere's surface); in the forcing scheme that is applied here, this is accomplished by imposing additional forces on the fluid at the surface of the primary spheres (which are then distributed to the lattice nodes in the vicinity of the particle surface). The details of the implementation of the forcing scheme can be found elsewhere.[23−25]

Determining Forces and Torques in Agglomerates. The collection of forces acting on the fluid at the surfaces of the primary spheres forming an agglomerate is used to determine the hydrodynamic force and torque acting on that agglomerate (action = −reaction). In addition to the hydrodynamic force and torque stemming from the LBM, the motion of the agglomerates is controlled by lubrication forces and by forces arising from the soft-sphere interactions that we use to deal with collisions between agglomerates. The equations of (linear and rotational) motion that we solve for an agglomerate consisting of n primary spheres can be written as

$$\begin{aligned} nm_0 \frac{\mathrm{d}\mathbf{v}_a}{\mathrm{d}t} &= \sum_{i=1}^{n} \mathbf{F}_i \\ \frac{\mathrm{d}\mathbf{L}_a}{\mathrm{d}t} &= \sum_{i=1}^{n} (\mathbf{T}_i + \mathbf{F}_i \times (\mathbf{r}_i - \mathbf{r}_a)) \\ \mathbf{L}_a &= \mathbf{I}_a \boldsymbol{\omega}_a \end{aligned} \tag{2}$$

with $\mathbf{v}_a$ and $\boldsymbol{\omega}_a$ being the linear and angular velocity of the agglomerate, $m_0 = \rho_s 4\pi/3a^3$ the mass of a primary sphere, and $\mathbf{L}_a$ and $\mathbf{I}_a$ the angular momentum vector and moment of inertia tensor of the agglomerate (see the Appendix for an expression in a Cartesian coordinate system of the latter). The vector $\mathbf{r}_i$ is the location of the center of sphere i. The torque $\mathbf{T}_i$ on primary sphere i directly follows from the LBM/forcing scheme.

As already indicated above, the force on primary sphere i ($\mathbf{F}_i$ in eq 2) has—in principle—three contributions: the hydrodynamic force stemming from the LBM (and forcing scheme), a radial lubrication force, and a soft-sphere interaction force which is also radial. The latter two contributions are nonzero only if a primary sphere belonging to another agglomerate is in close proximity of sphere i. Since they are radial, they do not contribute to the torque on the primary sphere.

The lubrication force is added as a hydrodynamic force in situations where two primary spheres belonging to different agglomerates are in close proximity and move relatively to one another. At some stage of proximity—typically when the surfaces of the two spheres involved are less than one grid spacing apart—the (fixed, i.e. nonadaptive) grid cannot accurately resolve the hydrodynamic interactions anymore and radial lubrication is explicitly added.[26] The expressions for the radial lubrication force are given in the Appendix.

A soft-sphere approach has been used to deal with collisions between primary spheres belonging to different agglomerates. The expressions for the soft-sphere force (which is also radial, it brings about smooth and fully elastic collisions) are also given in the Appendix.

The simulations provide us with the force and torque on each of the primary spheres ($\mathbf{F}_i$ and $\mathbf{T}_i$). From solving the set of equations in eq 2 we know the acceleration (linear and rotational) of the agglomerate as a whole so that we also know the acceleration, each primary sphere is undergoing:

$$\begin{aligned} \frac{\mathrm{d}\mathbf{v}_i}{\mathrm{d}t} &= \frac{\mathrm{d}\mathbf{v}_a}{\mathrm{d}t} + \frac{\mathrm{d}}{\mathrm{d}t}(\boldsymbol{\omega}_a \times (\mathbf{r}_i - \mathbf{r}_a)) \\ \frac{\mathrm{d}\boldsymbol{\omega}_i}{\mathrm{d}t} &= \frac{d\boldsymbol{\omega}_a}{\mathrm{d}t} \end{aligned} \tag{3}$$

As a consequence we can determine the force $\mathbf{F}_{c,i}$ and torque $\mathbf{T}_{c,i}$ required to keep each primary sphere attached to the agglomerate:

$$\begin{aligned} \mathbf{F}_{c,i} &= m_0 \frac{\mathrm{d}\mathbf{v}_i}{\mathrm{d}t} - \mathbf{F}_i \\ \mathbf{T}_{c,i} &= I_0 \frac{\mathrm{d}\boldsymbol{\omega}_a}{\mathrm{d}t} - \mathbf{T}_i \end{aligned} \tag{4}$$

(with $I_0 = (2/5)a^2 m_0$ the moment of inertia of the primary sphere about its center).

If primary sphere i has more than one contact point with other primary spheres in the agglomerate, $\mathbf{F}_{c,i}$ and $\mathbf{T}_{c,i}$ are the sum of contact forces and torques, respectively. In the general case of an agglomerate arbitrarily configured of equally sized, contacting spheres, it is not possible to determine the force and torque per contact point based on the collection of $\mathbf{F}_{c,i}$ and $\mathbf{T}_{c,i}$ values only: Solving for forces and torques per contact point poses an ill defined problem (analogous to static indeterminacy in structural analysis). Additional physics, e.g. related to solids deformations in the agglomerate under mechanical loading, is required to close the system of equations. Still, we consider the availability of the summed contact forces and torques per primary sphere to be useful information for assessing breakage probability.

However, in this paper, we will be considering three simple agglomerates for which the forces and torques per contact point can be determined directly based on $\mathbf{F}_{c,i}$ and $\mathbf{T}_{c,i}$ ($i = 1 \ldots n$): doublets, triplets, and quadruplets. The doublets have a single contact point, and the resulting $\mathbf{F}_{c,i}$ and $\mathbf{T}_{c,i}$ are the force and torque in that single contact. The triplets are arranged in a triangle with two contact points per primary sphere; the quadruplets are arranged in a tetrahedron with three contact points per primary sphere. In the Appendix, it is shown for the triplets and quadruplets that by making a few sensible assumptions the force (and torque) per contact point can be determined based on the set of $\mathbf{F}_{c,i}$ and $\mathbf{T}_{c,i}$ per primary sphere.

Calibration and Validation. In our simulations, the radius of each primary spherical particle is specified and the input radius refers to this radius scaled by the lattice spacing in the (uniform and cubic) computational grid. In the LBM simulations, as the spherical particle is represented by forces that are confined to a cubic grid, the input radius does not reflect the actual radius of the particle. A calibration procedure to estimate the effective radius of this object (commonly referred to as the hydrodynamic radius) was introduced by Ladd.[27] We apply this scheme to estimate the hydrodynamic radius of the particles. The hydrodynamic radius is recognized as a and is given in lattice units. In this study, the radius has been set to $a = 6$. Previously,[28] the effect of grid resolution has been checked for dense, fluidized suspensions consisting of spherical particles with radii 6, 8, and 12. The onset and propagation of instabilities (the key issue in that paper) were virtually independent of the resolution. Wave speeds at the various resolutions were within 6% and agreed (within experimental error) with measured wave speeds (experiments due to Duru et al.[29]).

Derksen[11] studied the effect of spatial resolution for sphere doublets in simple shear flow. Again results for spheres with radii 6, 8, and 12 were compared in terms of the interaction force and the doublet's rotation rate and showed excellent mutual

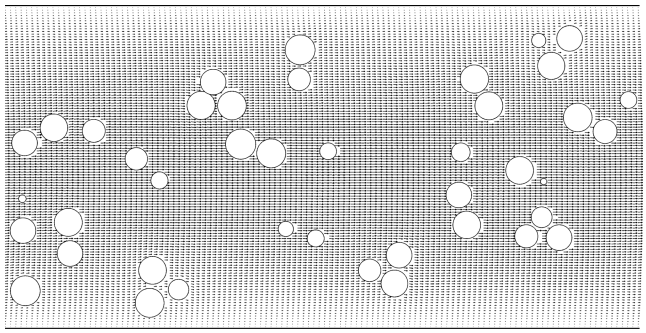

Figure 2. Velocity vector field in a cross section through the center of the uniform channel. Only 1 in 2 vectors in the streamwise direction are displayed. The circular disks represent the cross sections of the spherical particles in the same center plane. Quadruplets, $\phi = 0.093$.

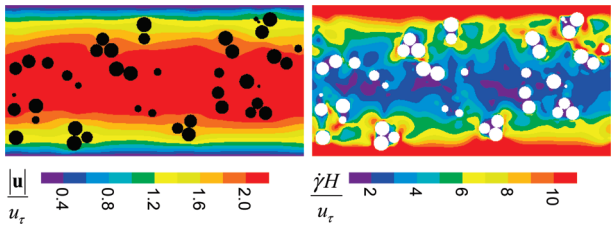

Figure 3. Contours of velocity magnitude (left) and deformation rate $\dot{\gamma}$ for the same realization as Figure 2.

agreement and excellent agreement with the analytical solution for creeping flow conditions due to the work of Nir and Acrivos.[12]

Numerical Settings. The spatial resolution of the simulations is fully defined by fixing the primary sphere radius a to 6 lattice distances. Given the uniform cubic grid and the fixed aspect ratios, the rest of the dimensions can be derived from this (e.g., the channel width H spans 120 lattice spacings since $a/H = 0.05$ throughout this work). The time step is such that the flow time scale $1/\dot{\gamma}_w \equiv \rho\nu/\tau_w$ amounts to 1320 time steps (in a time period of $1/\dot{\gamma}_w$, a fluid element near the center of a uniform channel travels typically $0.5H$). The simulations are started from a zero flow field. It then takes roughly $50/\dot{\gamma}_w$ for the multiphase flow system to fully develop. After that initialization period, we run the simulations in quasi-steady state for at least $150/\dot{\gamma}_w$ to collect statistical data. The cases with lower solids volume fractions were run longer to have a sufficient number of collisions for meaningful statistical analysis.

Results

Flow Field Impressions. The laminar nature of the flows we are studying is evident from the velocity vector plot related to a uniform channel as given in Figure 2. The presence of the agglomerates, however, adds fluctuations and small-scale structures to the overall flow. We see that more clearly if we plot the same instantaneous realization as shown in Figure 2 in terms of contours of the velocity magnitude, and in terms of the generalized deformation rate $\dot{\gamma} = (2d_{ij}d_{ij})^{1/2}$ (with $d_{ij} = 1/2(\partial u_j/\partial x_i + \partial u_i/\partial x_j)$ the deformation rate tensor) as is done in Figure 3 (left and right panel, respectively). It is important to see that the agglomerates do not experience a homogeneous deformation rate around them so that estimating flow-induced disruptive forces based on the deformation rate of the undisturbed flow (the flow without agglomerates) is a coarse approximation at best.

Obviously, with the same body force acting on the liquid, the flow rates in the channels reduce if a contraction is present;

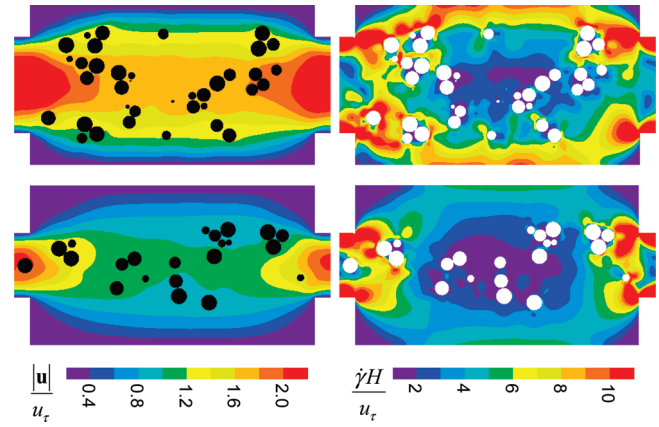

Figure 4. Contours of velocity magnitude (left) and deformation rate $\dot{\gamma}$ (right) for quadruplets in channels with contractions. (top) Contraction with $h/H = 0.2$. (bottom) $h/H = 0.3$. $\phi = 0.062$.

see Figure 4 (left panels). Therefore, compared to uniform channels at the same Reynolds number (and thus the same body force; see eq 1) contracted channels do not necessarily have higher overall (i.e., volume averaged) deformation rates. Deformation tends to increase locally as a result of the more complicated flow structure in a contracted channel and tends to decrease as a result of decreased flow rate and quiescent parts of the flow away from the contraction. Cleary, the contractions have strong impact on the spatial distribution of liquid deformation over the channel; compare the right panels of Figure 4 with the deformation field in Figure 3. We expect this to have impact on the forces experienced at the contact points of the primary spheres in the agglomerates.

Flow and Collision-Induced Forces in Agglomerates. During the simulations, we keep track of the entire force and torque history of every agglomerate so that we can reconstruct the contact forces and torques as a function of time, according to the procedures as explained in the Appendix. The discussion of the results in this paper focuses on the normal contact force. This is the projection of the contact force in the direction defined by the vector connecting the centers of the two spheres sharing the contact point under consideration. A tensile normal contact force is positive; a compressive normal contact force is negative. Note that the simulations provide us with the full (three-dimensional) contact force vectors and contact torque vectors for every contact point in every agglomerate at every moment in time. Which components and/or projections of forces and torques are critical for agglomerate breakage depends on the physics and/or chemistry of the bonds between the primary spheres forming the agglomerates. This is a subject beyond the scope of the present paper. The discussions regarding the normal contact force allow us to show the detailed level of information gathered by the simulations and to indicate some major trends in parameter space while not overloading the reader with the full (vectorial) contact force and torque information.

In Figure 5, we show samples of time series of the normal force. It has been nondimensionalized according to $F_n^* = F_n/(\mu\dot{\gamma}_w a^2)$, with $\dot{\gamma}_w = \tau_w/\mu$, with dimensionless time being $t^* = t\dot{\gamma}_w$. Each time series corresponds to one contact point in one single agglomerate. The top panel compares simulations with quadruplets at three solids volume fractions, the middle panel compares three channel layouts (again for quadruplets), and the bottom panel compares doublets, triplets, and quadruplets.

The smooth parts of the time series relate to the agglomerate translating and rotating through the laminar flow with a continuous change in the direct laminar hydrodynamic environ-

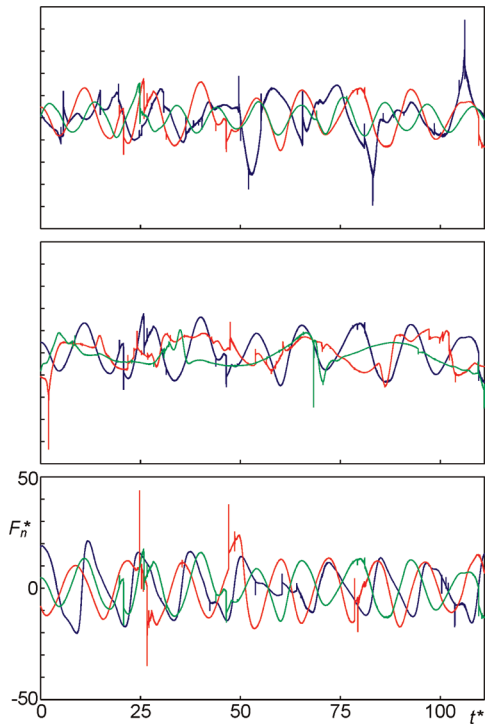

Figure 5. Time series of the normal force in a single point of contact. Force has been normalized according to $F_n^* = F_n/(\mu\dot{\gamma}_w a^2)$, and time was normalized according to $t^* = t\dot{\gamma}_w$ with $\dot{\gamma}_w = \tau_w/\mu$ the average wall shear rate. (top panel) Quadruplets in a uniform channel with solids volume fraction $\phi =$ 0.093 (blue curve), 0.062 (red), and 0.031 (green). (middle panel) Quadruplets at $\phi = 0.062$ in a uniform channel (blue), a channel with contraction $h/H = 0.2$ (red), and a channel with contraction $h/H = 0.3$ (green). (bottom panel) Doublets (blue), triplets (red), and quadruplets (green) in a uniform channel at $\phi = 0.062$. The ordinate has the same scale in all panels.

ment resulting in a gradual change in the normal force. The time scale of these smooth fluctuations is of the order of $10/\dot{\gamma}_w$. The spikes and apparent discontinuities in the force signal are due to collisions with other agglomerates in the channel.

Comparing the different time series obtained under different conditions and in different channels hints at a few trends. In the denser suspension, the agglomerate collides more frequently leading to a normal-force signal with more spikes (top panel of Figure 5). Also, the flow seen by the agglomerate is more complex in the denser suspension. This leads to the smooth fluctuations of the signal in the denser suspension having higher amplitude and higher frequencies. The effect of the contraction appears to be a reduction in the amplitude of the normal force (middle panel of Figure 5). The agglomerates passing through the contraction can be reconstructed from these time series. A low-frequency variation of the force signal is from time to time followed by faster fluctuations when the agglomerate passes through the contraction (e.g., during $31 < t^* < 34$ for $h/H =$ 0.3, i.e. the green curve). Comparing the force time series in doublets, triplets, and quadruplets does not indicate a clear trend. For this specific time series, triplets (red) show somewhat stronger force fluctuations than doublets and quadruplets.

In order to more quantitatively analyze the normal force data based on the full amount of information contained in the simulations, we condensed the normal forces in all contact points in all agglomerates at each moment in time in force probability density functions (PDF's) and organized them in Figure 6. Simulations at three solids volume fractions were performed in the uniform channel ($\phi =$ 0.093, 0.062, and 0.031); in the contracted channels two solids volume fractions (0.062 and 0.031) were considered. A number of interesting dependencies can be observed in the various panels of Figure 6 and by comparing the various panels presented there. An apparent trend relates to the solids volume fraction. The more agglomerates, the higher the chances for collisions and also the more vigorous the collisions (as visible in the upper panel of Figure 5) and thus the higher the chances for high normal force levels. As a result, the tails (high and low end) of the PDF's for the higher solids volume fractions lie systematically above those for the lower solids volume fractions. The exception is the lower left panel of Figure 6 (doublets in a strongly contracted channel) where the compressive forces in the $\phi = 0.031$ slurry are higher than those in the $\phi = 0.062$ agglomerate slurry.

The force PDF's of the different agglomerate types (doublets, triplets, and quadruplets) in the uniform (i.e., noncontracted) channels (top row of Figure 6) differ significantly. The (smaller) doublets have narrower PDF's than the triplets and quadruplets. The difference not only relates to size but also to shape. The doublets (at least the ones in the center portion of the channel) tend to align with the flow, specifically if the solids volume fraction is low so that collisions do not scatter the orientations. These effects reduce the chance of collisions and also reduce the (absolute value of) the contact force since the spheres in the aligned doublet see more or less the same hydrodynamic environment. There are minor differences between the force distributions of triplets and quadruplets.

Changing the channel geometry by placing contractions influences the flow-induced forces. For the quadruplets and the triplets, the trend is from more Gaussian-shaped distributions (quadratic on the lin-log-scale of Figure 6) for uniform channels toward exponential distributions (linear on lin-log-scale) for the strongest contractions. For the doublets, the trends as a result of contractions are less systematic; we do observe a widening of the normal force PDF as a result of placing a contraction.

Dimensionless force peak levels $F_n^* = F_n/(\mu\dot{\gamma}_w a^2)$ are of the order of 50 (see Figure 6). To place this number in context: in an undisturbed channel flow (i.e., the flow without solids), the wall shear rate $\dot{\gamma}_w = \tau_w/\mu$ is practically the highest shear rate encountered. That high-end shear rate would result in dimensionless force levels of $F_n^* \approx 20$.[11,12] That the actual peak levels are a factor of 2.5 higher than this estimate therefore is the result of the complexity of the flow as induced by the solids and the collisions between agglomerates.

Conclusions

Motivated by the potential role of liquid deformation in the breakage of agglomerates we have set up a computational procedure for determining flow-induced forces in agglomerates and applied it for three simple agglomerate configurations (doublets, triplets, and quadruplets all made of equally sized spheres) in laminar channel flow. The simulations fully resolve the liquid flow which is two-way coupled with the motion of the agglomerates. The flow simulations are based on lattice-Boltzmann discretization; collisions between agglomerates are based on a soft-sphere approach. During the simulations the agglomerates maintain their integrity and we keep track of the forces at the contact points required to keep the spheres, the agglomerates are made of, attached.

In terms of probability density functions (PDF's), the forces in the agglomerates depend on the solids volume fraction in the agglomerate slurry with increased chances for high force levels at high solids loading. This is largely due to increasing the collision probabilities in denser suspensions but also due to the more complex hydrodynamic environment of an agglomerate

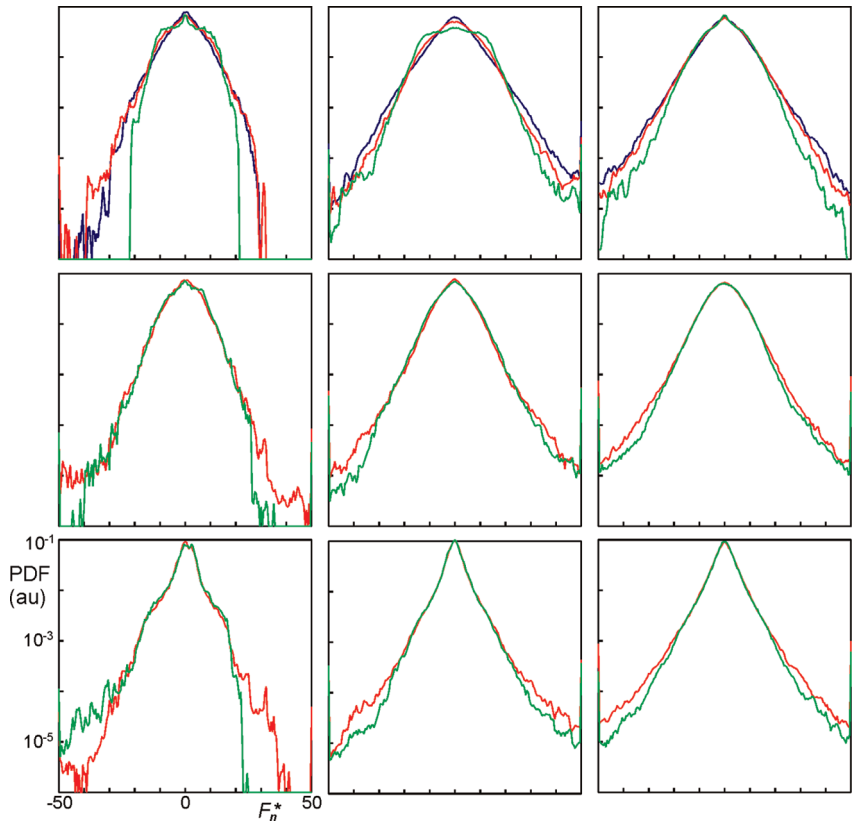

Figure 6. Probability density functions (PDF's) of the normal contact force. (from left to right) Doublets, triplets, and quadruplets. (from top to bottom) Uniform channel, contracted channel with $h/H = 0.2$, and contracted channel with $h/H = 0.3$. Blue curves have $\phi = 0.093$, red curves have $\phi = 0.062$, and green curves have $\phi = 0.031$. The abscissa and ordinate have the same scale in all panels.

in a dense suspension. Sphere doublets experience weaker normal forces compared to triplets and quadruplets.

We also investigated the impact of placing a contraction in the channel has on the flow-induced force levels. Sharp contractions have been used in experiments to promote agglomerate breakage.[14] In our study, contracted channels have been compared with uniform channels on the basis of equal pressure drop. This implies that the volumetric flow rate in the contracted channels is smaller than in uniform channels. Still (in general) the contracted channels widen the normal force PDF's hinting at their usefulness for promoting breakage.

Future work will be in applying the procedures for determining flow-induced forces in agglomerates to more generic flows, first and foremost homogeneous, isotropic turbulence. Such simulations will allow us to relate turbulence characteristics such as energy dissipation rate and Kolmogorov scale (relative to agglomerate size) with force and torque levels in agglomerates. This information would be useful for assessing breakage probabilities in turbulent, large-scale process equipment-size flows. Performing simulations with finite-strength agglomerates is another direction for future work. In such simulations, we actually would break agglomerates if certain threshold forces, torques, and/or stresses are exceeded. By specifying direct interparticle force fields, we could study and fully couple the interplay between agglomerate morphology and fluid flow.

Acknowledgment

Support of the Schlumberger DBR Technology Center is gratefully acknowledged.

Appendix

In this appendix, a few detailed issues regarding the mechanics of agglomerate motion and agglomerate interaction are discussed.

Agglomerate Moment of Inertia Tensor

The moment of inertia tensor $\mathbf{I}_a$ for an agglomerate consisting of n equally sized spheres with respect to its center of mass as used in eq 2 in Cartesian coordinates reads

$$\mathbf{I}_a = \sum_{i=1}^{n} \begin{bmatrix} I_0 + m_0(\Delta y_i^2 + \Delta z_i^2) & -m_0 \Delta x_i \Delta y_i & -m_0 \Delta x_i \Delta z_i \\ -m_0 \Delta x_i \Delta y_i & I_0 + m_0(\Delta x_i^2 + \Delta z_i^2) & -m_0 \Delta y_i \Delta z_i \\ -m_0 \Delta x_i \Delta z_i & -m_0 \Delta y_i \Delta z_i & I_0 + m_0(\Delta x_i^2 + \Delta y_i^2) \end{bmatrix} \tag{A1}$$

with Δx_i, Δy_i, and Δz_i the components of the vector $\mathbf{r}_i - \mathbf{r}_a$, i.e. the vector connecting the center of primary sphere i and the center of mass of the agglomerate, $m_0 = \rho_s(4\pi/3)a^3$, and $I_0 = (2/5)a^2 m_0$.

Radial Lubrication Sphere−Sphere Interaction

If two solid spheres of the same size (radius a) and relative position $\mathbf{r}_{12} = \mathbf{r}_1 - \mathbf{r}_2$ move with relative velocity $\mathbf{u}_{12} = \mathbf{u}_1 - \mathbf{u}_2$ through a liquid with viscosity $\mu = \rho\nu$, the leading order term for the radial lubrication force on sphere 1 is[26,30]

$$\mathbf{F}_{lub1} = -3\pi\mu a^2(\mathbf{u}_{12} \cdot \mathbf{r}_{12})\frac{1}{s}\frac{\mathbf{r}_{12}}{|\mathbf{r}_{12}|^2} \tag{A2}$$

with s being the distance between the sphere surfaces ($s = |\mathbf{r}_{12}| - 2a$). An opposite force acts on sphere 2. This leading order term scales with a/s. Subsequent terms are of order $\ln(a/s)$ and of lower order.[30]

When implementing eq A2 in a lattice-Boltzmann framework, we need to deal with two issues. In the first place, the lubrication force only needs to be switched on when s gets of the order of—or smaller than—the lattice spacing. If s is larger, the LBM effectively deals with the hydrodynamic interactions between the spheres and explicitly adding the lubrication force is not required. We follow the approach due to Nguyen and Ladd:[26] instead of eq A2, we write

$$\mathbf{F}_{\text{lubl}} = -3\pi\mu a^2(\mathbf{u}_{12}\cdot\mathbf{r}_{12})\left(\frac{1}{s} - \frac{1}{s_0}\right)\frac{\mathbf{r}_{12}}{|\mathbf{r}_{12}|^2} \qquad \text{if } s \le s_0$$
$$\mathbf{F}_{\text{lubl}} = \mathbf{0} \qquad \text{if } s > s_0 \tag{A3}$$

If the *numerical* parameter s_0 is chosen as $0.2a$, radial lubrication is recovered accurately.[28]

In the second place, we prevent the lubrication force from becoming singular by saturating it when s gets below a threshold value δ, here chosen as $\delta = 2 \times 10^{-4}a$. Earlier results[28] show that overall results are not sensitive to this choice.

Soft-Sphere Interactions

The soft-sphere interaction model used to mimic sphere−sphere collisions has two parameters: the distance δ_0 between two sphere surfaces at which a repulsive force is switched on and a spring constant k. The expression for the soft-sphere related force on sphere 1 is

$$\mathbf{F}_{\text{ss1}} = k(\delta_0 - s)\frac{\mathbf{r}_{12}}{|\mathbf{r}_{12}|} \qquad \text{if } s \le \delta_0$$
$$\mathbf{F}_{\text{ss1}} = \mathbf{0} \qquad \text{if } s > \delta_0 \tag{A4}$$

By choosing $\delta_0 = 0.015a$ and $k = 0.75(u_\tau^2/\delta_0^2)\rho_s(4\pi/3)a^3$ (the latter implies that the work done by the soft-sphere related force acting from $s = \delta_0$ to $s = 0$ is 0.75 times the kinetic energy of a sphere traveling with the wall-shear velocity which is a characteristic velocity of the flow system), we hardly have any overlap of spheres; if overlap occurs it is always less than $0.01a$. Furthermore, the collisions are elastic and frictionless. The latter was confirmed by achieving energy conservation when doing dry granular simulations (i.e., simulations without interstitial liquid) with a number of spheres having u_τ as rms velocity.

Sphere−wall interactions were dealt with in a similar manner as sphere−sphere interactions, i.e. by using an expression similar to eq A4. The force now points in the wall-normal direction, s is the distance between sphere surface and wall, for δ_0 we took $0.0075a$, and k was the same as for the sphere−sphere contacts.

Forces and Torques Per Contact Point for Triplets and Quadruplets

Triplets. The triplets are arranged in a triangle; see Figure A1. From our simulations, we know $\mathbf{F}_{c,i}$ and $\mathbf{T}_{c,i}$, $i = 1, 2, 3$. From these, we want to determine the forces and torques at the points of contact, i.e. $\mathbf{F}_A$, $\mathbf{F}_B$, $\mathbf{F}_C$ and $\mathbf{T}_A$, $\mathbf{T}_B$, $\mathbf{T}_C$. In three dimensions, there are 18 unknowns. The equations we have available express the fact that $\mathbf{F}_{c,i}$ and $\mathbf{T}_{c,i}$ ($i = 1, 2, 3$) stem from forces and torques at the contact points:

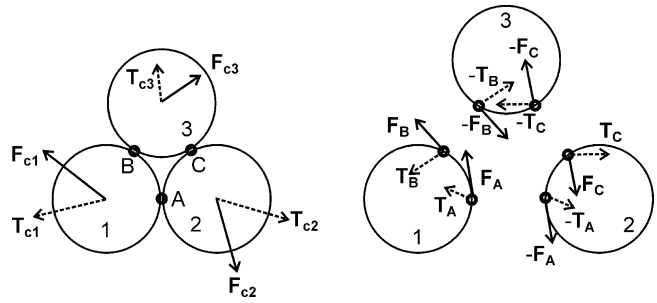

Figure A1. Definition of triplets, the forces $\mathbf{F}_{c,i}$, and torques $\mathbf{T}_{c,i}$ to keep the primary spheres attached, and the forces $\mathbf{F}_A$, $\mathbf{F}_B$, and $\mathbf{F}_C$ and torques $\mathbf{T}_A$, $\mathbf{T}_B$, and $\mathbf{T}_C$ acting at the contact points. All forces and torques (in general) have three dimensions; for clarity, the two-dimensional projections are shown.

$$\mathbf{F}_A + \mathbf{F}_B = \mathbf{F}_{c1} \quad -\mathbf{F}_A + \mathbf{F}_C = \mathbf{F}_{c2} \quad -\mathbf{F}_B - \mathbf{F}_C = \mathbf{F}_{c3}$$
$$\mathbf{T}_A + \mathbf{T}_B - \mathbf{F}_A\frac{\mathbf{r}_{12}}{2} - \mathbf{F}_B\frac{\mathbf{r}_{13}}{2} = \mathbf{T}_{c1}$$
$$-\mathbf{T}_A + \mathbf{T}_C - \mathbf{F}_A\frac{\mathbf{r}_{12}}{2} - \mathbf{F}_C\frac{\mathbf{r}_{23}}{2} = \mathbf{T}_{c2}$$
$$-\mathbf{T}_B - \mathbf{T}_C - \mathbf{F}_B\frac{\mathbf{r}_{13}}{2} - \mathbf{F}_C\frac{\mathbf{r}_{23}}{2} = \mathbf{T}_{c3} \tag{A5}$$

Since $\sum_{i=1}^{3}\mathbf{F}_{c,i} = \mathbf{0}$ and $\sum_{i=1}^{3}\mathbf{T}_{c,i} = \mathbf{0}$, the equations are not independent; we only have two independent force equations and two independent torque equations leading (in 3D) to 12 linearly independent equations in the 18 unknown force and torque components in the contact points A, B, and C. We "close" the system by assuming that the contact point torques $\mathbf{T}_A$, $\mathbf{T}_B$, and $\mathbf{T}_C$ only have a bending component in the plane defined by the three sphere center points, the rationale being that torques in the other two directions (torsion and bending in the plane's normal direction) are not necessarily required to keep the integrity of the agglomerate, contact forces are able to ascertain integrity. This reduces the number of unknowns to 12 for which we have 12 linear equations that we solve.

Quadruplets. The quadruplets are arranged in a tetrahedron so that each of the four spheres is in contact with the other three. There is a total of 6 contact points and thus a total of 36 unknowns (being the components of the contact forces and torques). In analogy to triplets, we can set up three (the number of spheres minus one) independent force and torque equations, making a total of 18 equations. In the quadruplets, we close the set of equations by setting all torque components equal to zero. Compared to the triplets, the extra sphere in the quadruplets makes that also the in-plane bending torque component can be taken care of by contact forces. We then only have 18 (unknown) contact forces that we solve with the 18 equations.

Literature Cited

(1) Hounslow, M. J.; Mumtaz, H. S.; Collier, A. P.; Barrick, J. P.; Bramley, A. S. A. Micro-mechanical model for the rate of aggregation during precipitation from solution. *Chem. Eng. Sci.* **2001**, *56*, 2543.

(2) Hollander, E. D.; Derksen, J. J.; Portela, L. M.; Van den Akker, H. E. A. A numerical scale-up study for orthokinetic agglomeration in stirred vessels. *AIChE J.* **2001**, *47*, 2425.

(3) Guerrero-Sanchez, C.; Erdmenger, T.; Ereda, P.; Wouters, D.; Schubert, U. S. Water-soluble ionic liquids as novel stabilizers in suspension polymerization reactions: Engineering polymer beads. *Chemistry−A* **2006**, *12*, 9036.

(4) Selomulya, C.; Bushell, G.; Amal, R.; Waite, T. D. Aggregation Mechanisms of Latex of Different Particle Sizes in a Controlled Shear Environment. *Langmuir* **2002**, *18*, 1974.

(5) Mody, N. A.; Lomakin, O.; Doggett, T. A.; Diacovo, T. G.; King, M. R. Mechanics of transient platelet adhesion to von Willebrand factor under flow. *Biophys. J.* **2005**, *88*, 1432.

(6) Pierce, F.; Sorensen, C. M.; Chakrabarti, A. Aggregation-Fragmentation in a Model of DNA-Mediated Colloidal Assembly. *Langmuir* **2005**, *21*, 8992.

(7) Boek, E. S.; Ladva, H. K.; Crawshaw, J. P.; Padding, J. T. Deposition of Colloidal Asphaltene in Capillary Flow: Experiments and Mesoscopic Simulation. *Energy Fuels* **2008**, *22*, 805.

(8) Rahmani, N. H. G.; Masliyah, J. H.; Dabros, T. Characterization of Asphaltenes Aggregation and Fragmentation in a Shear Field. *AIChE J.* **2003**, *49*, 1645.

(9) Hounslow, M. J.; Reynolds, G. K. Product engineering for crystal size distribution. *AIChE J.* **2006**, *52*, 2507.

(10) Aamir, E.; Nagy, Z. K.; Rielly, C. D.; Kleinert, T.; Judat, B. Combined quadrature method of moments and method of characteristics approach for efficient solution of population balance models for dynamic modeling and crystal size distribution control of crystallization processes. *Ind. Eng. Chem. Res.* **2009**, *48*, 8575.

(11) Derksen, J. J. Flow induced forces in sphere doublets. *J. Fluid Mech.* **2008**, *608*, 337.

(12) Nir, A.; Acrivos, A. On the creeping motion of two arbitrary-sized touching spheres in a linear shear field. *J. Fluid Mech.* **1973**, *59*, 209.

(13) Bäbler, M. U.; Morbidelli, M.; Bałdyga, J. Modelling the breakup of solid aggregates in turbulent flows. *J. Fluid Mech.* **2008**, *612*, 261.

(14) Zaccone, A.; Soos, M.; Lattuada, M.; Wu, H.; Bäbler, M. U.; Morbidelli, M. Breakup of dense colloidal aggregates under hydrodynamic stresses. *Phys. Rev. E* **2009**, *79*, 061401.

(15) Soos, M.; Ehrl, L.; Bäbler, M. U.; Morbidelli, M. Aggregate breakup in a contracting nozzle. *Langmuir* **2010**, *26*, 10.

(16) Higashitani, K.; Iimura, K.; Sanda, H. Simulation of deformation and breakup of large aggregates in flows of viscous fluids. *Chem. Eng. Sci.* **2001**, *56*, 2927.

(17) Becker, V.; Schlauch, E.; Behr, M.; Briesen, H. Restructuring of colloidal aggregates in shear flows and limitations of the free-draining approximation. *J. Colloid Interface Sc.* **2009**, *339*, 362.

(18) Eggersdorfer, M. L.; Kadau, D.; Herrmann, H. J.; Pratsinis, S. E. Fragmentation and restructuring of soft-agglomerates under shear. *J. Colloid Interface Sc.* **2010**, *342*, 261.

(19) Chen, S.; Doolen, G. D. Lattice Boltzmann method for fluid flows. *Annu. Rev. Fluid Mech.* **1998**, *30*, 329.

(20) Succi, S. *The lattice Boltzmann equation for fluid dynamics and beyond*; Clarendon Press: Oxford, 2001.

(21) Somers, J. A. Direct simulation of fluid flow with cellular automata and the lattice-Boltzmann equation. *App. Sci. Res.* **1993**, *51*, 127.

(22) Qian, Y. H.; d'Humieres, D.; Lallemand, P. Lattice BGK for the Navier-Stokes equations. *Europhys. Lett.* **1992**, *17*, 479.

(23) Goldstein, D.; Handler, R.; Sirovich, L. Modeling a no-slip flow boundary with an external force field. *J. Comput. Phys.* **1993**, *105*, 354.

(24) Derksen, J.; Van den Akker, H. E. A. Large-eddy simulations on the flow driven by a Rushton turbine. *AIChE J.* **1999**, *45*, 209.

(25) Ten Cate, A.; Nieuwstad, C. H.; Derksen, J. J.; Van den Akker, H. E. A. PIV experiments and lattice-Boltzmann simulations on a single sphere settling under gravity. *Phys. Fluids* **2002**, *14*, 4012.

(26) Nguyen, N.-Q.; Ladd, A. J. C. Lubrication corrections for lattice-Boltzmann simulations of particle suspensions. *Phys. Rev. E* **2002**, *66*, 046708.

(27) Ladd, A. J. C. Numerical simulations of particle suspensions via a discretized Boltzmann equation. Part I: Theoretical Foundation. *J. Fluid Mech.* **1994**, *271*, 285.

(28) Derksen, J. J.; Sundaresan, S. Direct numerical simulations of dense suspensions: wave instabilities in liquid-fluidized beds. *J. Fluid Mech.* **2007**, *587*, 303.

(29) Duru, P.; Nicolas, M.; Hinch, J.; Guazelli, E. Constitutive laws in liquid-fluidized beds. *J. Fluid Mech.* **2002**, *452*, 371.

(30) Kim, S.; Karrila, S. J. *Microhydrodynamics: Principles and Selected Applications*; Butterworth-Heinemann: Woburn, MA, 1991.

Received for review February 27, 2010
Revised manuscript received April 3, 2010
Accepted April 9, 2010

IE100442E